Cell Reports, Volume *34*

Supplemental Information

D614G Mutation Alters SARS-CoV-2 Spike Conformation and Enhances Protease Cleavage at the S1/S2 Junction

Sophie M.-C. Gobeil, Katarzyna Janowska, Shana McDowell, Katayoun Mansouri, Robert Parks, Kartik Manne, Victoria Stalls, Megan F. Kopp, Rory Henderson, Robert J. Edwards, Barton F. Haynes, and Priyamvada Acharya

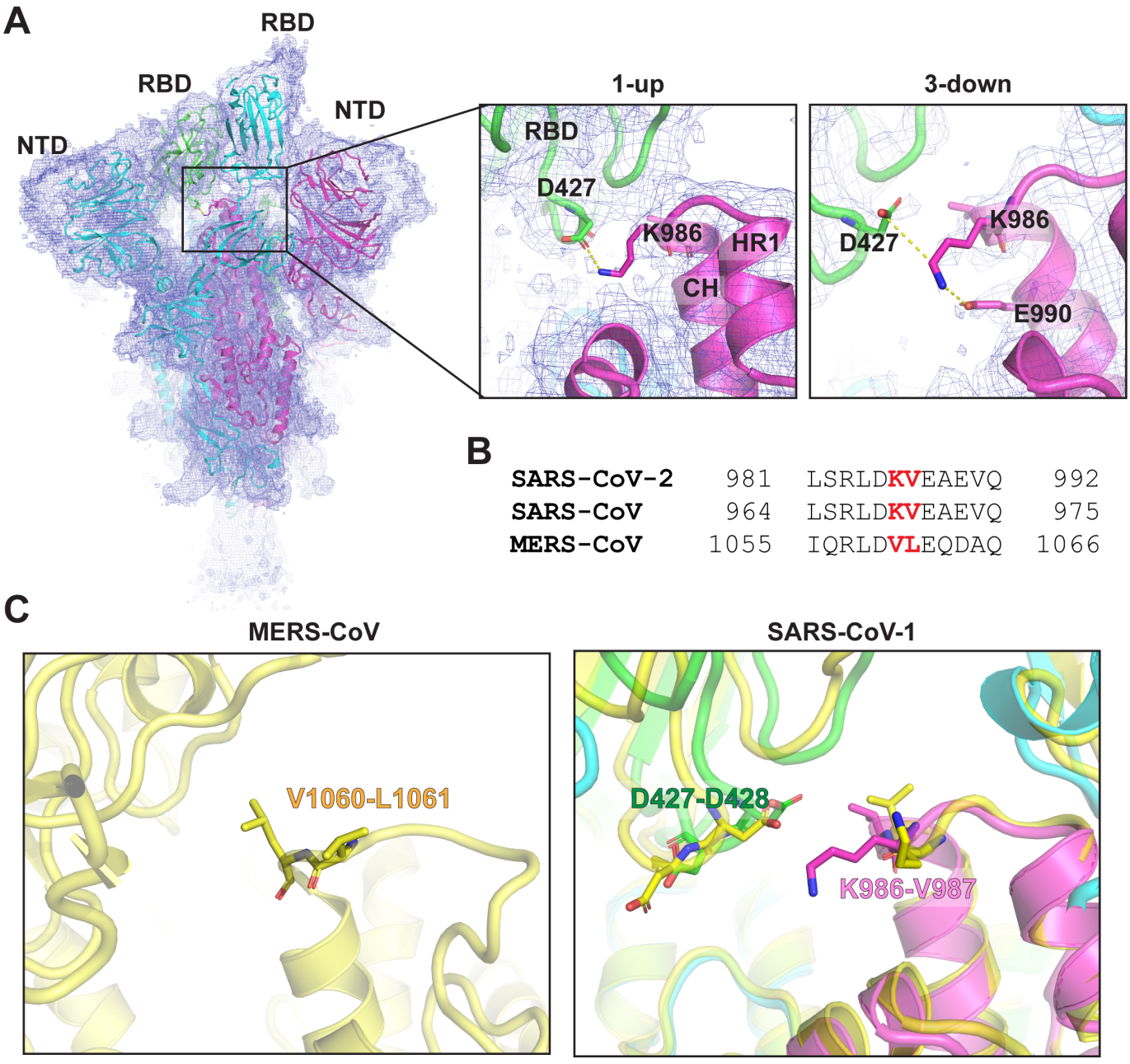

Figure S1. Structural comparison of residues 986-987 in the SARS-CoV-2 S ectodomain with the MERS and SARS-CoV-1 S ectodomains, Related to Figure 2. A. Cryo-EM reconstruction map of the 1-RBD-up states of the SARS-CoV-2 S-GSAS ectodomain (EMDB-22822; PDB ID 7KDH) colored by chains and zoomed-in view of residues K986-V987 in the 1-RBD-up and 3-RBD-down structures. The cryo-EM map is shown as a transparent surface and the fitted model is in cartoon representation, with residues shown as balls and sticks. **B.** Sequence alignment of residues 981-992 of SARS-CoV-2 and corresponding residues of SARS-CoV-1 and MERS spike proteins. **C.** Magnified view of one protomer showing residues V1060 and L1061 from MERS (PDB 5X5C; in yellow) and SARS-CoV-1 (PDB 5X58; in yellow) overlayed with residues K986 and V987 from SARS-CoV-2 S-GSAS ectodomain (colored as in **A**).

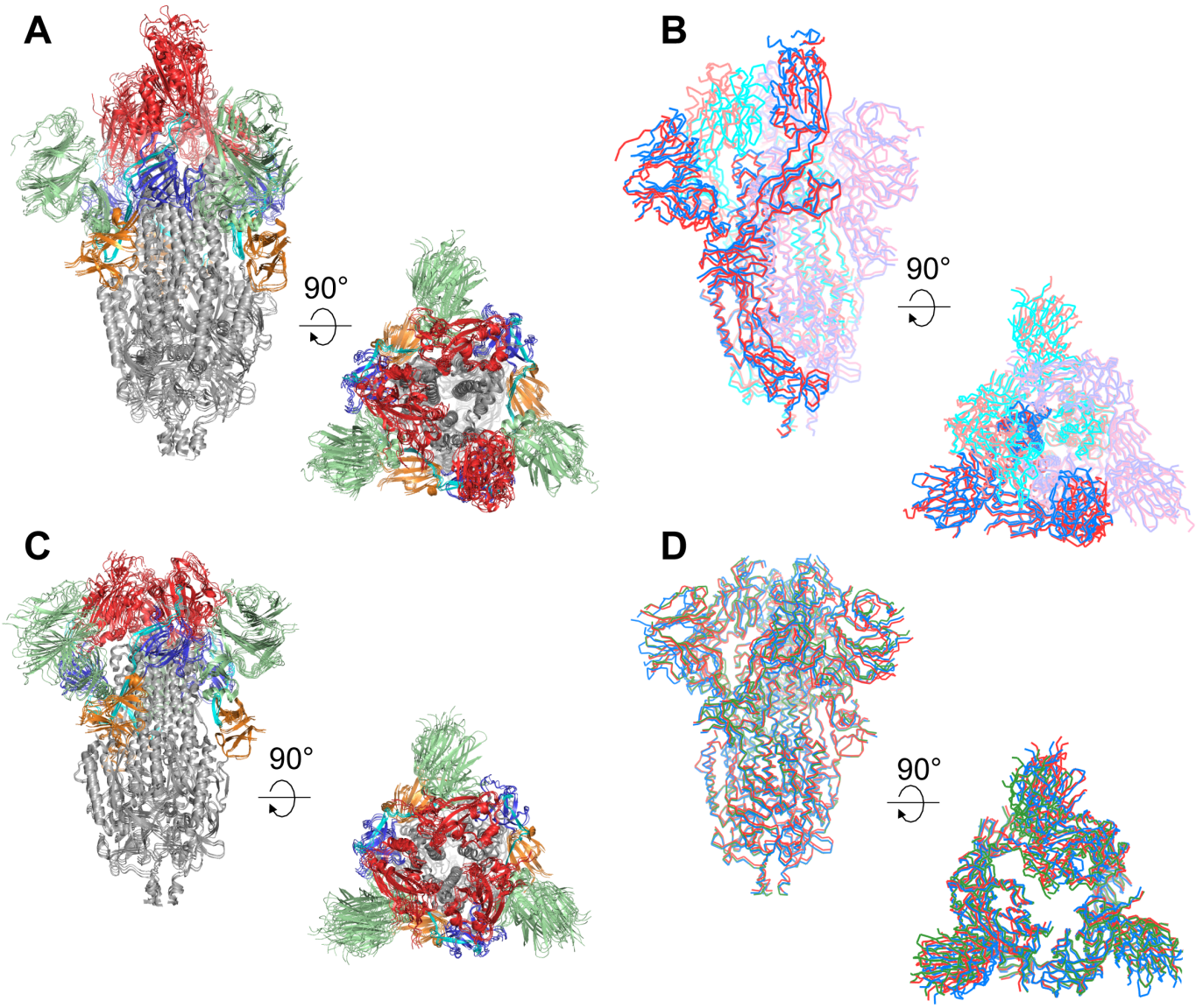

Figure S2. Overlay of the S-GSAS/D614G 1-up and 3-down substates, Related to Figure 3. Side and top view of the superposition of the **A.** 1-up substate structures of S-GSAS/D614G from Figure **3D** (PDB ID 7KE9, 7KEA, 7KEB and 7KEC) and **C.** of the 3-down substate structures (PDB ID 7KE4, 7KE6, 7KE7 and 7KE8) from Figure **3E.** The structures were superimposed using S2 subunit residues 908-1035 (spanning the HR1 and CH regions) with the S1 subunit colored by domain and the S2 subunit colored grey. RBD is colored red, NTD green, SD1 dark blue, SD2 orange and the linker between the NTD and RBD colored cyan. **B.** Ribbon representation of the overlay of the 1-up substate structures of S-GSAS/D614G colored by chain (PDB ID 7KE9 and 7KEC). **D.** Ribbon representation of the overlay of the 3-down substate structures of S-GSAS/D614G colored by state (PDB ID 7KE4, 7KE7 and 7KE8).

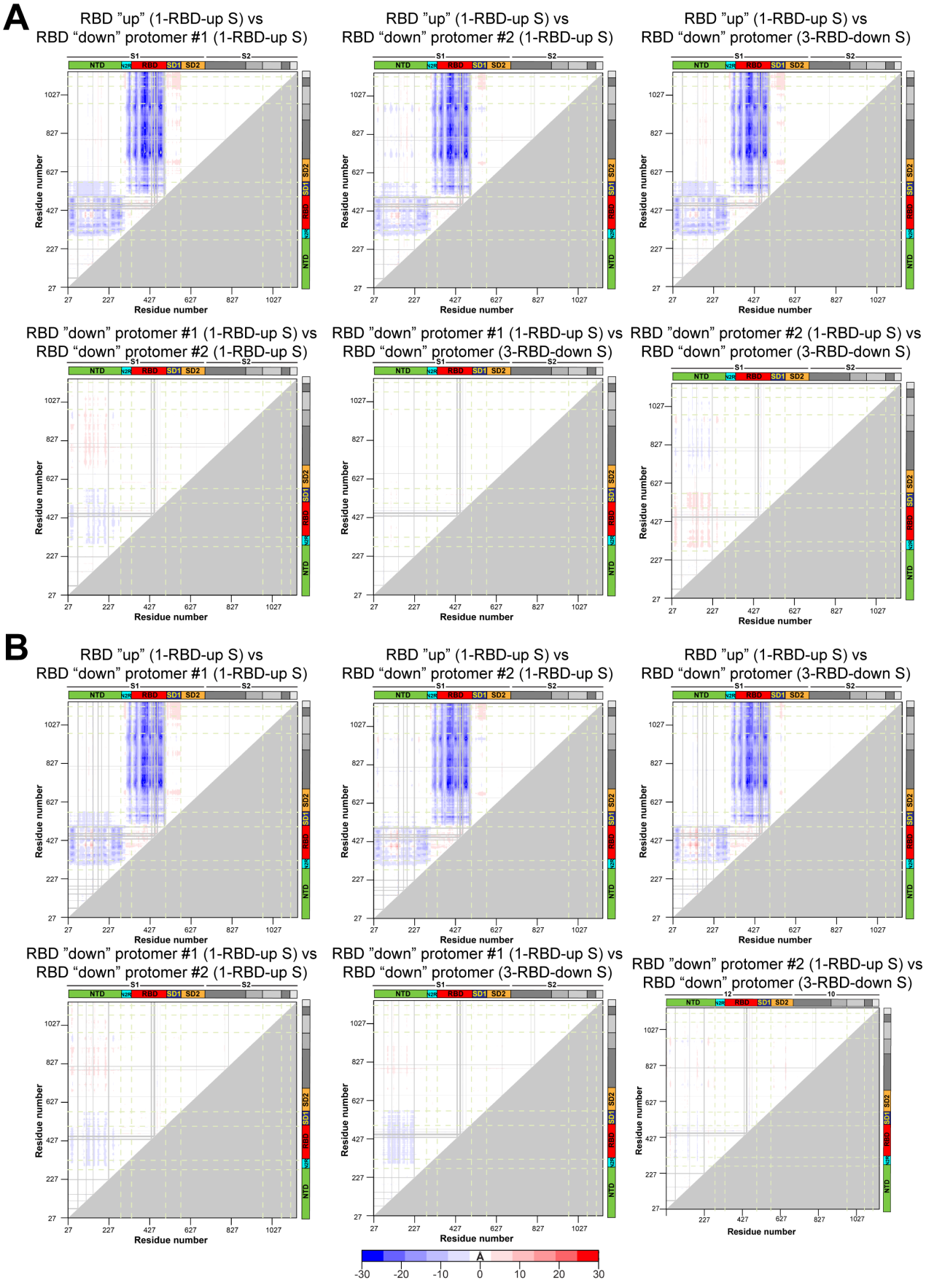

Figure S3. Difference distance matrices (DDM) analysis of S-GSAS and S-RRAR/D614G fully cleaved by furin showing structural changes between different protomers, Related to Figure 4. The S-GSAS DDM are shown in **A** and S-RRAR/D614G in **B**. The blue to white to red coloring scheme is illustrated at the bottom.

Table S1. Cryo-EM data collection and refinements statistics for the S-GSAS, S-GSAS/D614G and furin cleaved S-RRAR/D614G SARS-CoV-2 spike ectodomains, Related to Figures 2, 3 and 7.

	S-GSAS		S-GSAS/D614G Consensus		S-RRAR/D614G Furin cleaved	
	3-down	1-up	3-down	1-up	3-down	1-up
PDB ID	7KDG	7KDH	7KDK	7KDL	7KDI	7KDJ
EMDB ID	22821	22822	22825	22826	22823	22824
Data collection and processing						
Microscope	FEI Titan Krios					
Detector	Gatan K3					
Magnification	81,000		81,000		81,000	
Voltage (kV)	300		300		300	
Electron exposure (e–/Å2)	65.24		51.8		65.94	
Defocus range (μm)	0.8-2.5		0.40-2.94		0.38-2.88	
Pixel size (Å)	1.069		1.058		1.058	
Reconstruction software	cryoSparc					
Symmetry imposed	C3	C1	C3	C1	C3	C1
Initial particle images (no.)	2,566,724		2,343,150		479,208	
Final particle images (no.)	581,495	175,529	782,485	613,271	224,310	99,165
Map resolution (Å)	3.01	3.33	2.8	2.96	3.26	3.49
FSC threshold	0.143	0.143	0.143	0.143	0.143	0.143
Refinement						
Initial model used	6VXX	6VYB	6VXX	6VYB	6VXX	6VYB
Model resolution (Å)	3.01	3.33	2.8	2.96	3.26	3.49
FSC threshold	0.143	0.143	0.143	0.143	0.143	0.143
Map sharpening B factor (Å^2)	-129.3	-101.3	-121.5	-106.9	-104.2	-94.8
Model composition						
Nonhydrogen atoms	23,700	22,698	23,688	22,365	23,688	22,365
Protein residues	2,916	2,891	2,916	2,875	2,916	2,875
R.m.s. deviations						
Bond lengths (Å)	0.013	0.012	0.013	0.012	0.012	0.012
Bond angles (°)	1.845	1.838	1.87	1.835	1.789	1.757
Validation						
MolProbity score	1.03	1.13	0.98	0.96	0.97	1.03
Clashscore	0.28	0.43	0.3	0.09	0.15	0.23
Poor rotamers (%)	0.31	0.56	0.12	0.27	0.27	0.44
Ramachandran plot						
Favored (%)	93.46	92.3	94.66	93.6	93.81	93.21
Allowed (%)	6.22	7.31	5.24	6.11	6.12	6.4
Disallowed (%)	0.32	0.39	0.11	0.29	0.07	0.39

Table S1 continued. Cryo-EM data collection and refinements statistics for the S-GSAS, S-GSAS/D614G and furin cleaved S-RRAR/D614G SARS-CoV-2 spike protein ectodomains, Related to Figures 2, 3 and 7.

	S-GSAS/D614G Substates							
	3-down				1-up			
PDB ID	7KE4	7KE6	7KE7	7KE8	7KE9	7KEA	7KEB	7KEC
EMDB ID	22831	22832	22833	22834	22835	22836	22837	22838
Data collection and processing								
Magnification	81,000							
Voltage (kV)	300							
Electron exposure (e–/Å^2)	51.8							
Defocus range (μm)	0.40-2.94							
Pixel size (Å)	1.058							
Symmetry imposed	C1							
Initial particle images (no.)	2,343,150							
Final particle images (no.)	182,326	196,173	157,254	133,373	287,765	145,566	127,429	58,580
Map resolution (Å)	3.21	3.1	3.32	3.26	3.08	3.33	3.48	3.84
FSC threshold	0.143	0.143	0.143	0.143	0.143	0.143	0.143	0.143
Refinement								
Initial model used	6VXX	6VXX	6VXX	6VXX	6VYB	6VYB	6VYB	6VYB
Model resolution (Å)	3.21	3.1	3.32	3.26	3.08	3.33	3.48	3.84
FSC threshold	0.143	0.143	0.143	0.143	0.143	0.143	0.143	0.143
Map sharpening B factor (Å^2)	-95.3	-98.8	-92.8	-91.2	-104.5	-88.9	-86.2	-81
Model composition								
Nonhydrogen atoms	23,684	23,688	23,688	23,684	22,365	22,365	22,365	22,337
Protein residues	2,916	2,916	2,916	2,916	2,875	2,875	2,875	2,875
R.m.s. deviations								
Bond lengths (Å)	0.013	0.013	0.013	0.013	0.012	0.012	0.012	0.012
Bond angles (°)	1.845	1.838	1.81	1.836	1.813	1.893	1.856	1.845
Validation								
MolProbity score	1.02	1	1.1	1.13	0.95	1.23	1.3	1.58
Clashscore	0.13	0.15	0.34	0.41	0.11	0.64	0.83	0.74
Poor rotamers (%)	1.06	1.02	0.08	1.1	0.04	1.24	0.13	2.44
Ramachandran plot								
Favored (%)	92.93	93.25	92.23	92.9	93.99	92.42	90.31	89.92
Allowed (%)	6.72	6.47	7.49	6.82	5.79	7.15	9.08	9.05
Disallowed (%)	0.35	0.28	0.28	0.28	0.21	0.43	0.61	1.04

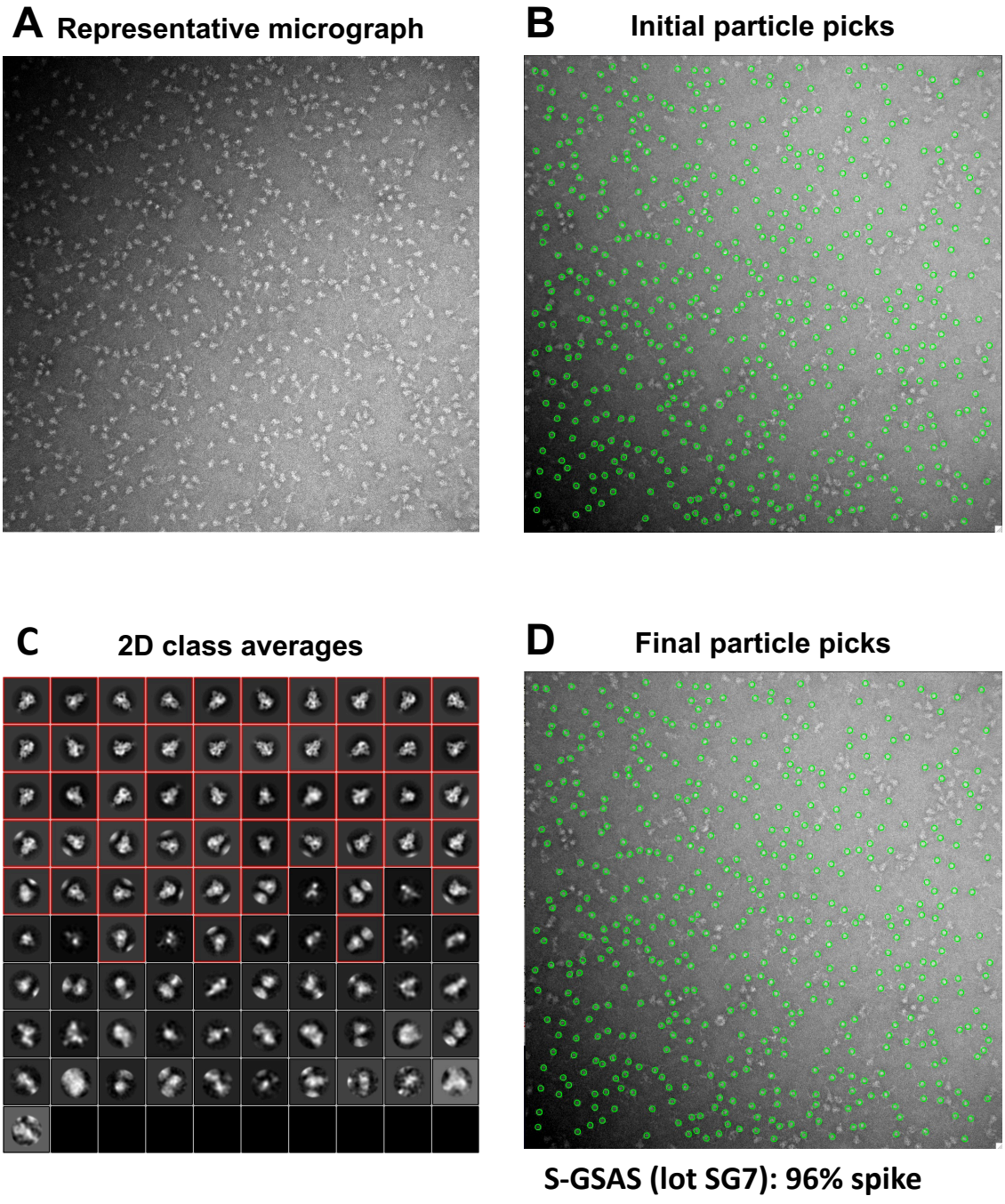

Data S1. NSEM and Cryo-EM data processing for the S-GSAS SARS-CoV-2 S ectodomain, Related to Figure 2. A. Representative NSEM micrograph. **B**. NSEM Particle picks in green. **C**. 2D class averages; the particles in the classes marked with a red box are recognizable as the pre-fusion spike. The rest of the classes are marked as "junk". **D**. NSEM Particles present in the boxed class averages in panel **C.** are shown with a green circle around them.

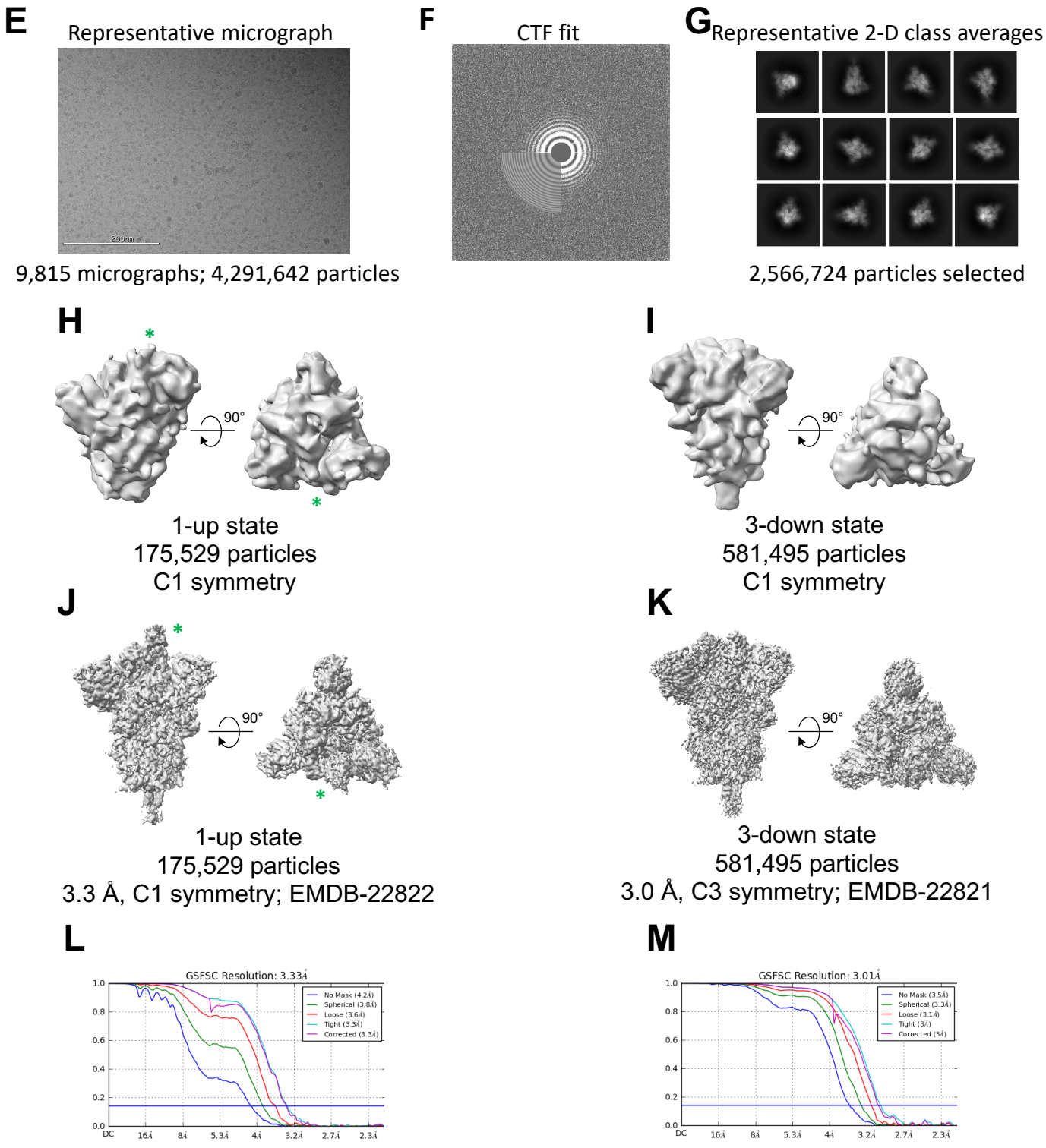

Data S1 continued. NSEM and Cryo-EM data processing for the S-GSAS SARS-CoV-2 S ectodomain, Related to Figure 2. E. Representative cryo-EM micrograph. **F**. Cryo-EM CTF fit. **G**. Representative 2D class averages from Cryo-EM dataset. **H-I.** *Ab initio* reconstructions for the cryo-EM **H**. 1-up state (the RBD in the up position is identified by an asterisk) and **I.** 3-down state. **J-K**. Refined maps for the cryo-EM **J.** 1-up state (the RBD in the up position is identified by an asterisk) and **K.** 3-down state. **L-M.** Fourier shell correlation curves for the cryo-EM **L.** 1-up state and **M.** 3-down state.

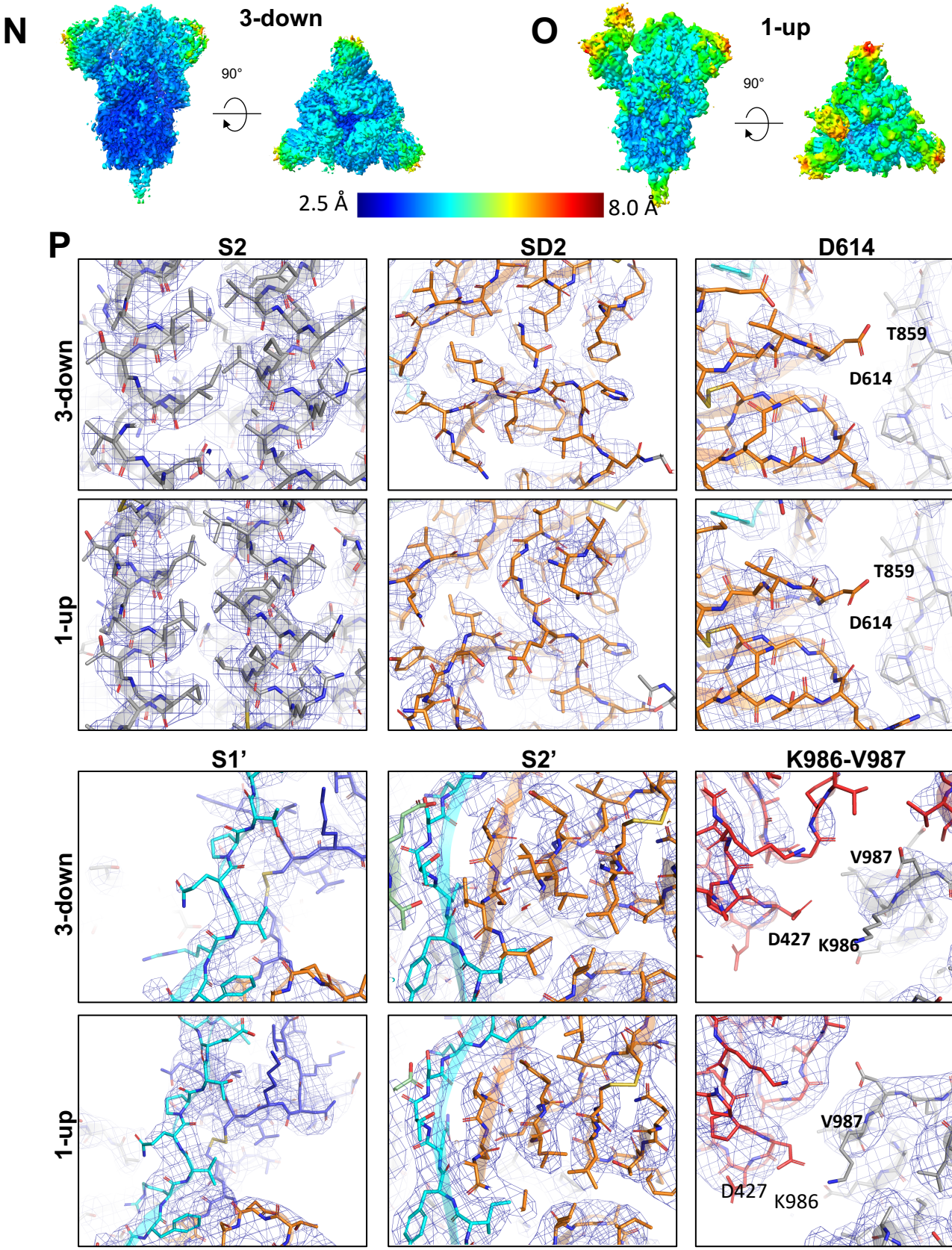

Data S1 continued. NSEM and Cryo-EM data processing for the S-GSAS SARS-CoV-2 S ectodomain, Related to Figure 2. N-O. Refined cryo-EM maps colored by local resolution for the **N.** 3-RBD-down (EMDB-22821) and **O.** 1-RDB-up (EMD-22822) states. **P.** Zoom-in images showing the S2, SD2, D614, S1', S2' and K986-V987 regions in the 3-RBD-down (top) and 1-RDB-up structures (bottom). The cryo-EM map is shown as a transparent surface and the fitted model is in cartoon representation, with residues shown as balls and sticks (PDB ID 7KDG and 7KDH).

Data S1. NSEM and Cryo-EM data processing for the S-GSAS SARS-CoV-2 S ectodomain, Related to Figure 2. A. Representative NSEM micrograph. **B.** NSEM Particle picks in green. **C.** 2D class averages; the particles in the classes marked with a red box are recognizable as the pre-fusion spike. The rest of the classes are marked as "junk". **D.** NSEM Particles present in the boxed class averages in panel C. are shown with a green circle around them. **E.** Representative cryo-EM micrograph. **F.** Cryo-EM CTF fit. **G.** Representative 2D class averages from Cryo-EM dataset. **H-I.** *Ab initio* reconstructions for the cryo-EM **H.** 1-up state (the RBD in the up position is identified by an asterisk) and **I.** 3-down state. **J-K.** Refined maps for the cryo-EM **J.** 1-up state (the RBD in the up position is identified by an asterisk) and **K** 3-down state. **L-M.** Fourier shell correlation curves for the cryo-EM **L.** 1-up state and **M.** 3-down state. **N-O.** Refined cryo-EM maps colored by local resolution for the **N.** 3-RBD-down (EMDB-22821) and **O.** 1-RDB-up (EMD-22822) states. **P.** Zoom-in images showing the S2, SD2, D614, S1', S2' and K986-V987 regions in the 3-RBD-down (top) and 1-RDB-up structures (bottom). The cryo-EM map is shown as a transparent surface and the fitted model is in cartoon representation, with residues shown as balls and sticks (PDB ID 7KDG and 7KDH).

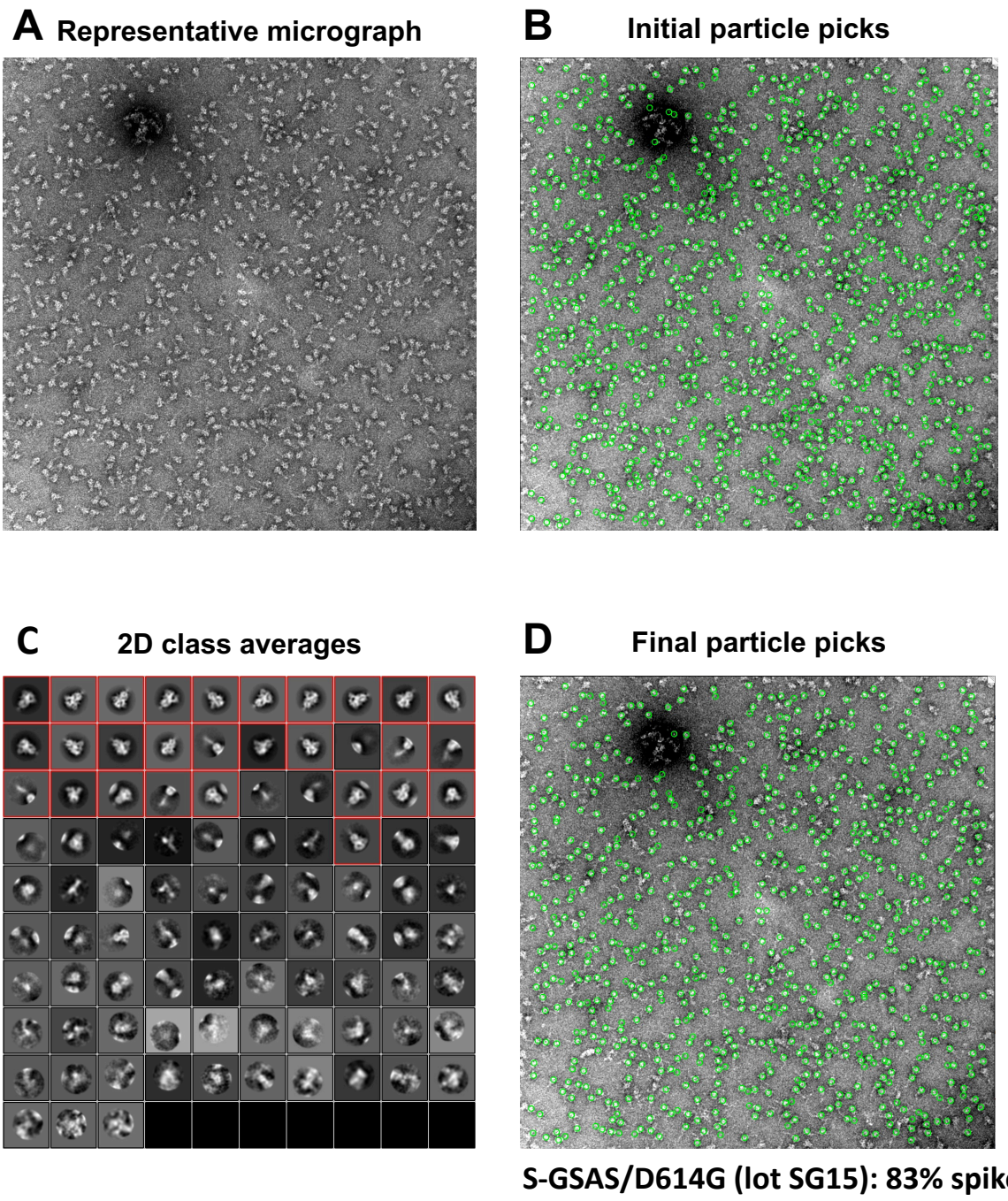

Data S2. NSEM and Cryo-EM data processing for the S-GSAS/D614G ectodomain consensus structures, Related to Figure 3. A. Representative NSEM micrograph. **B.** NSEM Particle picks in green. **C.** 2D class averages; the particles in the classes marked with a red box are recognizable as the pre-fusion spike. The rest of the classes are marked as "junk". **D.** NSEM Particles present in the boxed class averages in panel **C**. are shown with a green circle around them.

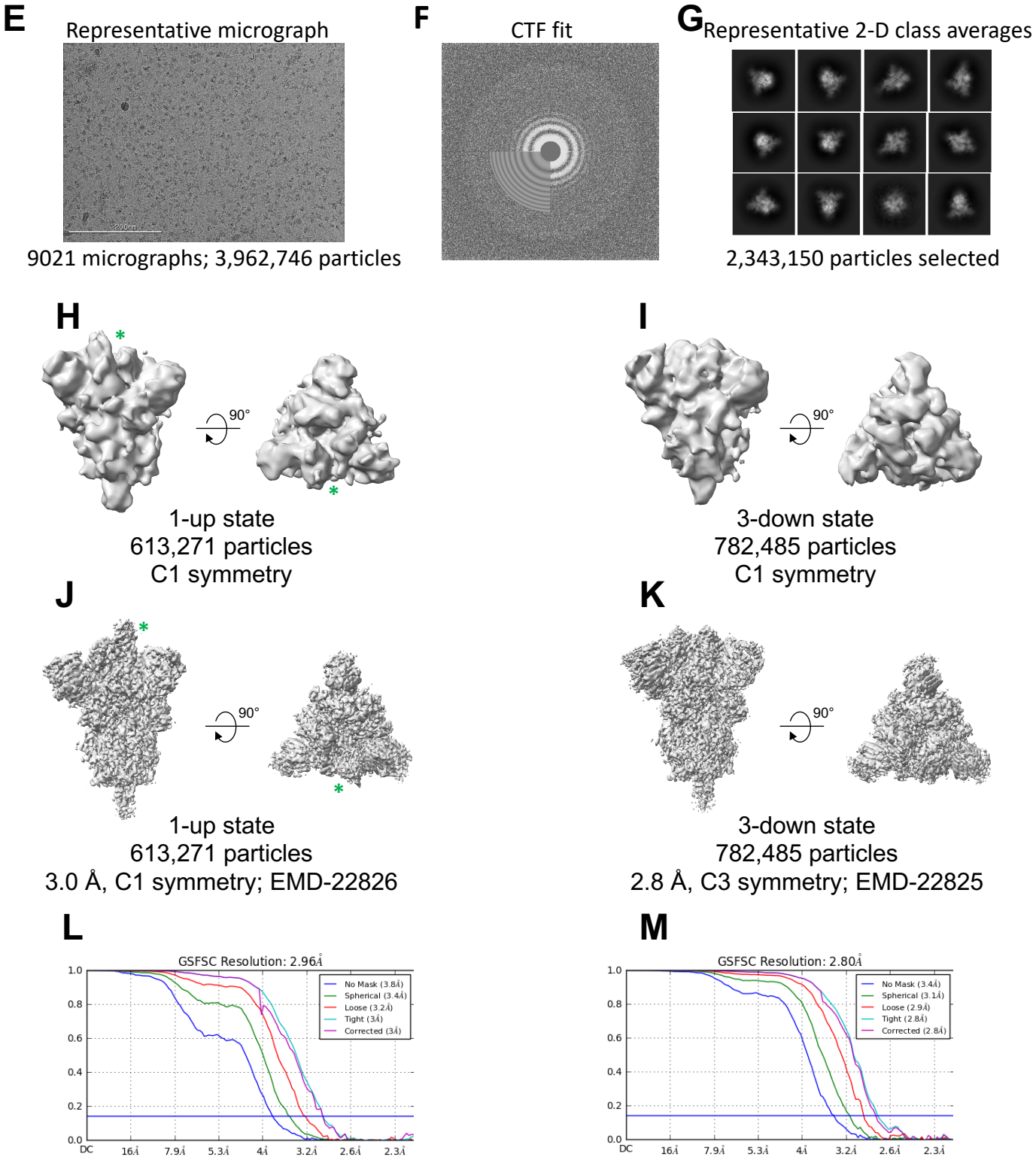

Data S2 continued. NSEM and Cryo-EM data processing for the S-GSAS/D614G ectodomain consensus structures, Related to Figure 3. E. Representative cryo-EM micrograph. **F.** Cryo-EM CTF fit. **G.** Representative 2D class averages from Cryo-EM dataset. **H-I.** *Ab initio* reconstructions for the cryo-EM **H.** 1-up state (the RBD in the up position is identified by an asterisk) and **I.** 3-down state. **J-K.** Refined maps for the cryo-EM **J.** 1-up state (the RBD in the up position is identified by an asterisk) and **K** 3-down state. **L-M.** Fourier shell correlation curves for the cryo-EM **L.** 1-up state and **M.** 3-down state.

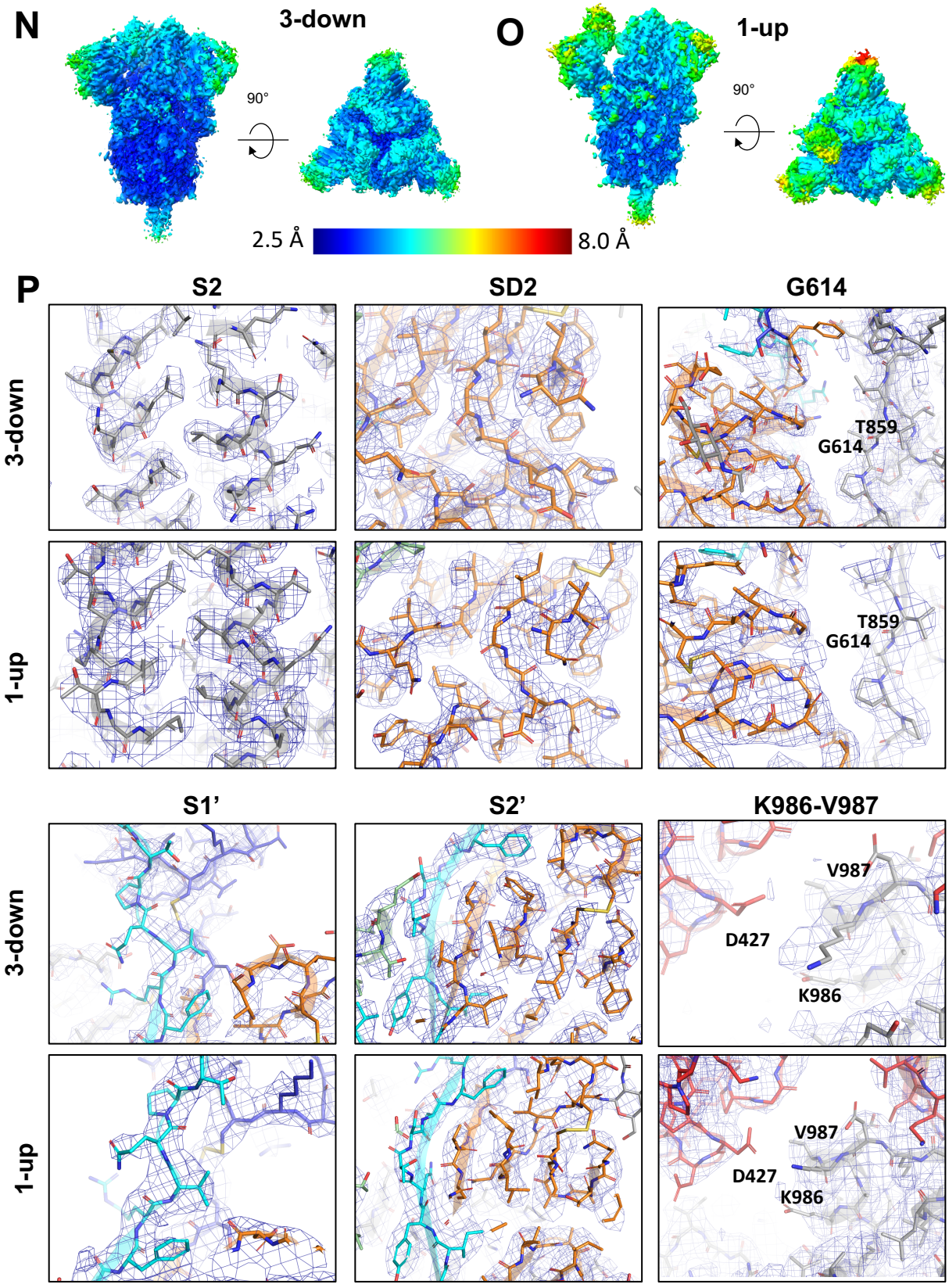

Data S2 continued. NSEM and Cryo-EM data processing for the S-GSAS/D614G ectodomain consensus structures, Related to Figure 3. N-O. Refined cryo-EM maps colored by local resolution for the consensus **N.** 3-RBD-down (EMDB-22825) and **O.** 1-RDB-up (EMD-22826) states. **P.** Zoom-in images showing the S2, SD2, D614, S1', S2' and K986-V987 regions in the consensus 3-RBD-down (top) and 1-RDB-up structures (bottom). The cryo-EM map is shown as a transparent surface and the fitted model is in cartoon representation, with residues shown as balls and sticks (PDB ID 7KDK and 7KDL).

Data S2. NSEM and Cryo-EM data processing for the S-GSAS/D614G ectodomain consensus structures, Related to Figure 3. A. Representative NSEM micrograph. **B.** NSEM Particle picks in green. **C.** 2D class averages; the particles in the classes marked with a red box are recognizable as the pre-fusion spike. The rest of the classes are marked as "junk". **D.** NSEM Particles present in the boxed class averages in panel **C**. are shown with a green circle around them. **E.** Representative cryo-EM micrograph. **F.** Cryo-EM CTF fit. **G.** Representative 2D class averages from Cryo-EM dataset. **H-I.** *Ab initio* reconstructions for the cryo-EM **H.** 1-up state (the RBD in the up position is identified by an asterisk) and **I.** 3-down state. **J-K.** Refined maps for the cryo-EM **J.** 1-up state (the RBD in the up position is identified by an asterisk) and **K** 3-down state. **L-M.** Fourier shell correlation curves for the cryo-EM **L.** 1-up state and **M.** 3-down state. **N-O.** Refined cryo-EM maps colored by local resolution for the consensus **N.** 3-RBD-down (EMDB-22825) and **O.** 1-RDB-up (EMD-22826) states. **P.** Zoom-in images showing the S2, SD2, D614, S1', S2' and K986-V987 regions in the consensus 3-RBD-down (top) and 1-RDB-up structures (bottom). The cryo-EM map is shown as a transparent surface and the fitted model is in cartoon representation, with residues shown as balls and sticks (PDB ID 7KDK and 7KDL).

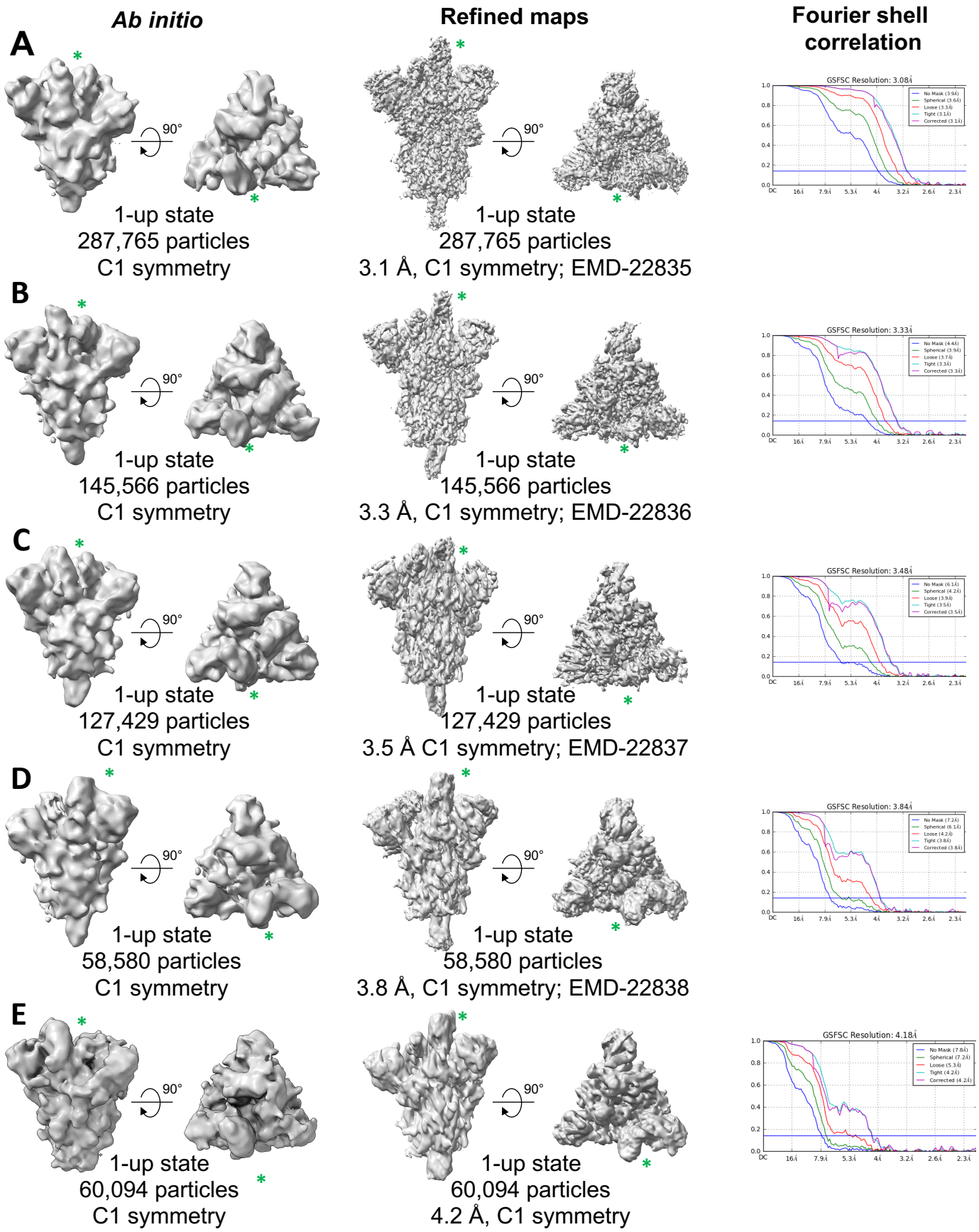

Data S3. Cryo-EM data processing details for S-GSAS/D614G 1-up and 3-down subpopulations, Related to Figure 3D and E. A-E. *Ab initio* reconstructions, refined maps and Fourier shell correlation curves for the 1-up subpopulations (the RBD in the up position is identified by an asterisk).

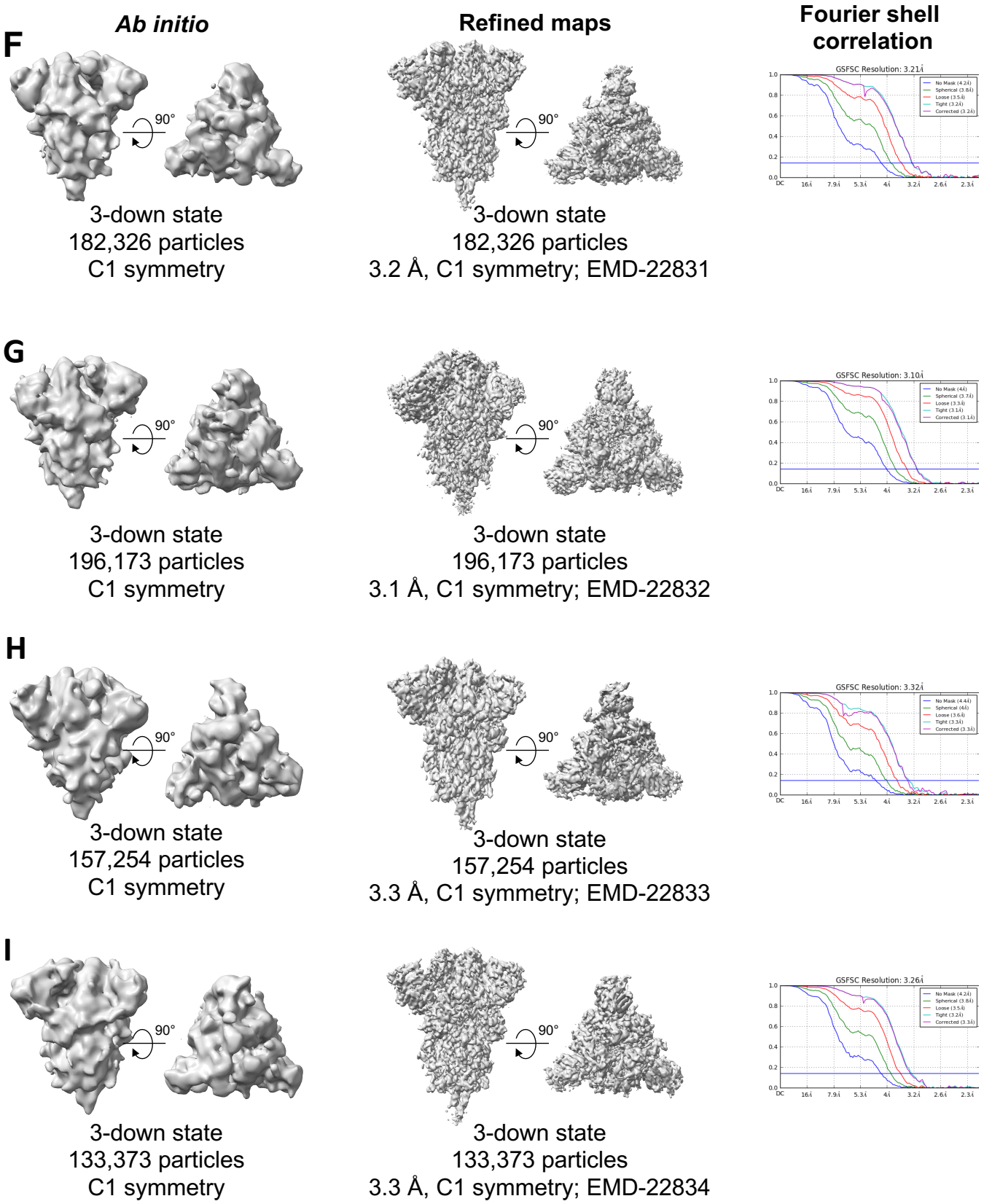

Data S3 continued. Cryo-EM data processing details for S-GSAS/D614G 1-up and 3-down subpopulations, Related to Figure 3D and E. F-K. *Ab initio* reconstructions, refined maps and Fourier shell correlation curves for the 3-down subpopulations.

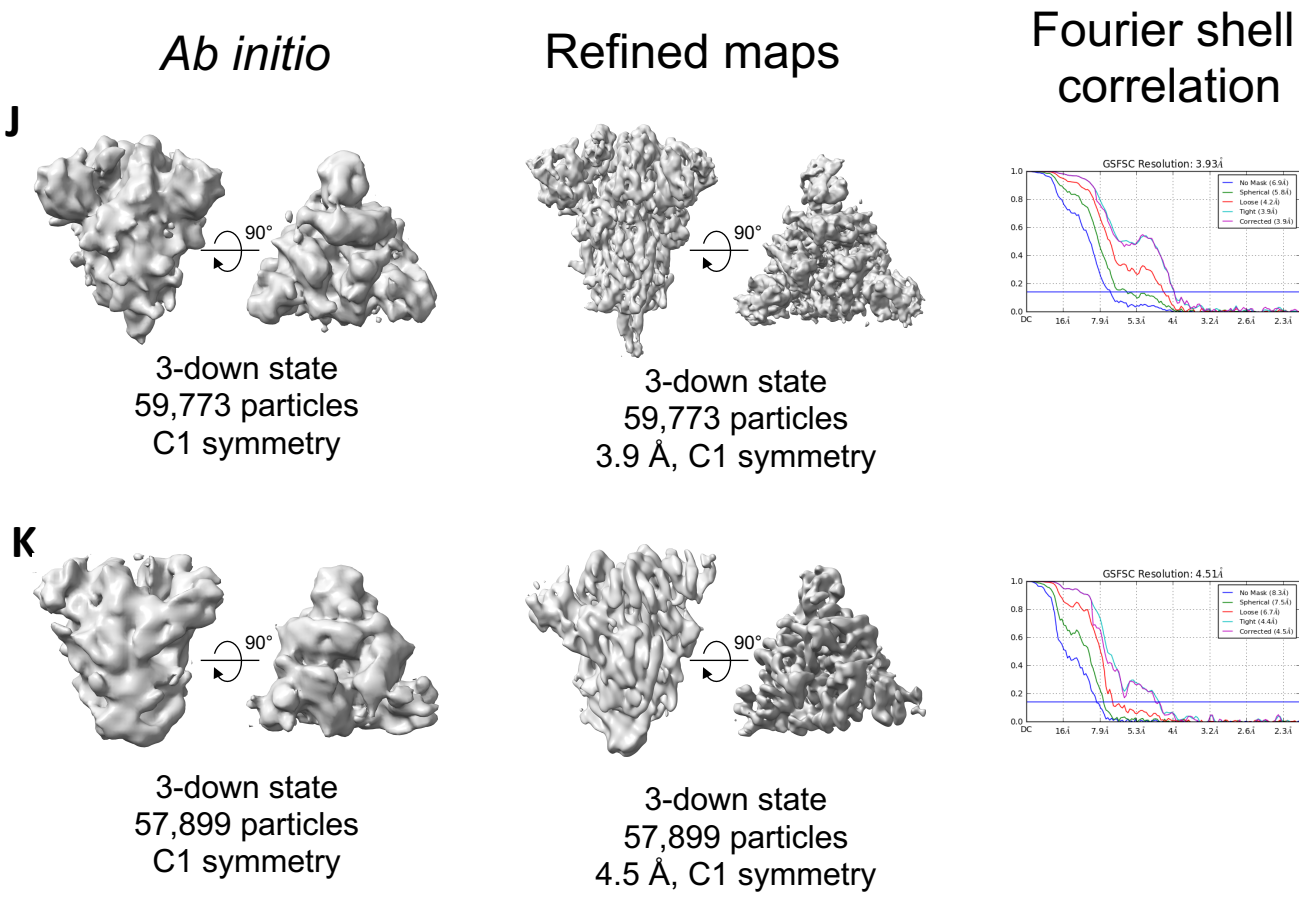

Data S3 continued. Cryo-EM data processing details for S-GSAS/D614G 1-up and 3-down subpopulations, Related to Figure 3D and E. F-K. *Ab initio* reconstructions, refined maps and Fourier shell correlation curves for the 3-down subpopulations.

Data S3. Cryo-EM data processing details for S-GSAS/D614G 1-up and 3-down subpopulations, Related to Figure 3D and E. A-E and overlay of the S-GSAS/D614G 1-up and 3-down substates. *Ab initio* reconstructions, refined maps and Fourier shell correlation curves for the 1-up subpopulations (the RBD in the up position is identified by an asterisk). **F-K.** *Ab initio* reconstructions, refined maps and Fourier shell correlation curves for the 3-down subpopulations.

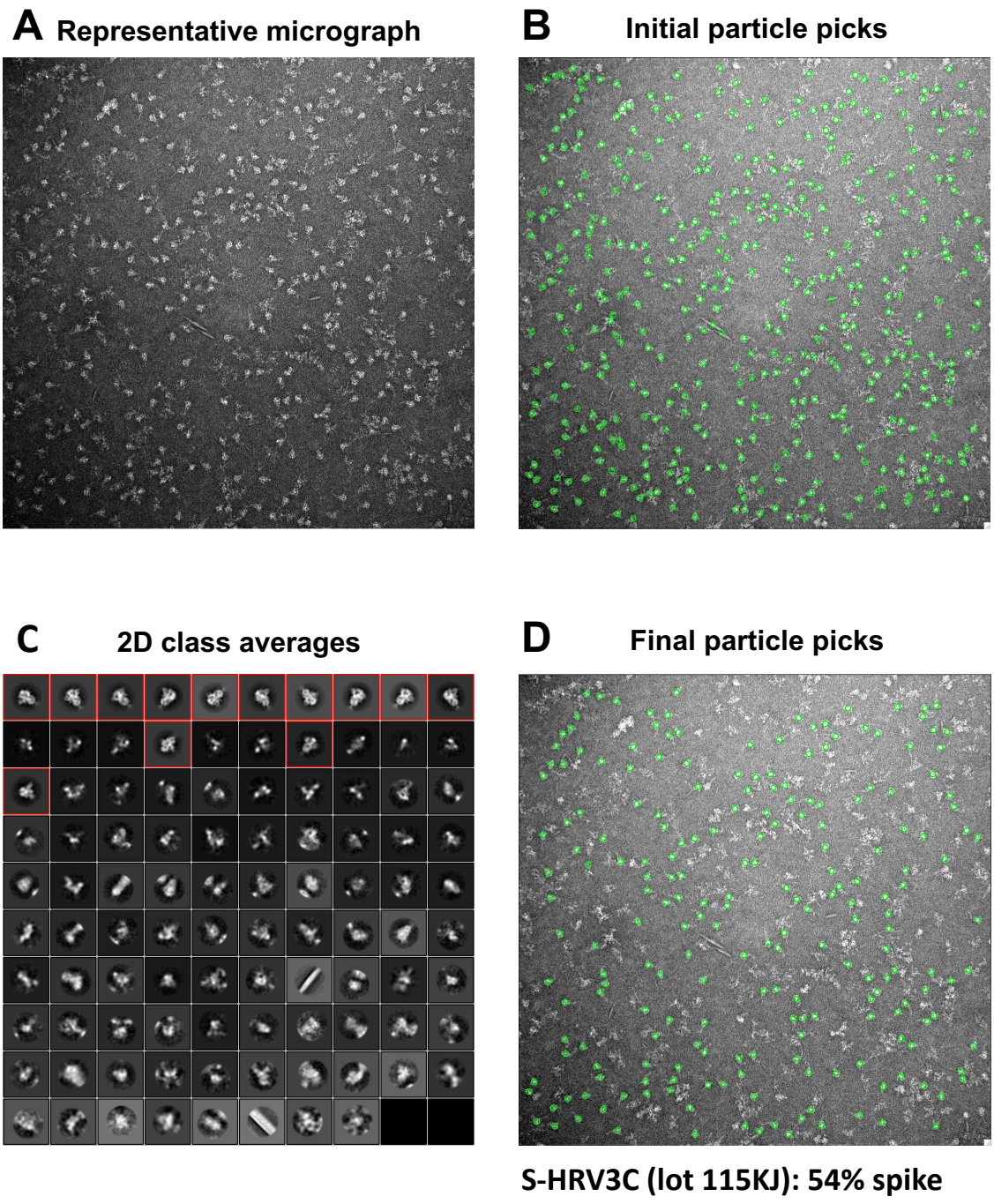

Data S4. NSEM quality control workflow for the S-HRV3C and S-HRV3C/D614G SARS-CoV-2 S ectodomains, Related to Figure 5. A and E. Representative NSEM micrograph of **A.** S-HRV3C and **E.** S-HRV3C/D614G SARS-CoV-2 S ectodomains. **B and F.** Particle picks in green. **C and G.** 2D class averages; the particles in the classes marked with a red box are recognizable as the pre-fusion spike. The rest of the classes are marked as "junk". **D and H.** Particles present in the boxed class averages in panel C. are shown with a green circle around them.

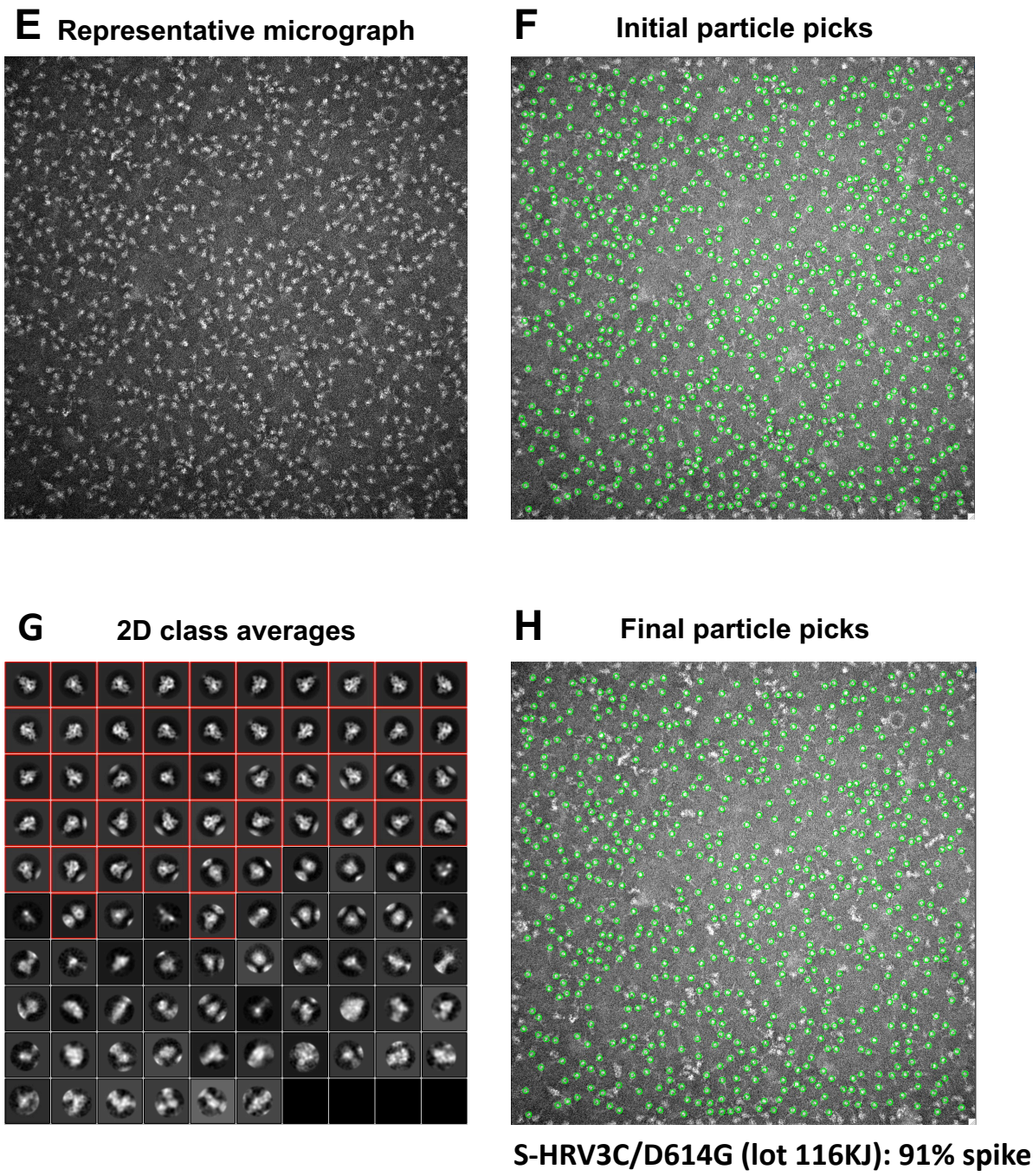

Data S4 continued. NSEM quality control workflow for the S-HRV3C and S-HRV3C/D614G SARS-CoV-2 S ectodomains, Related to Figure 5. A and E. Representative NSEM micrograph of **A.** S-HRV3C and **E.** S-HRV3C/D614G SARS-CoV-2 S ectodomains. **B and F.** Particle picks in green. **C and G.** 2D class averages; the particles in the classes marked with a red box are recognizable as the pre-fusion spike. The rest of the classes are marked as "junk". **D and H.** Particles present in the boxed class averages in panel C. are shown with a green circle around them.

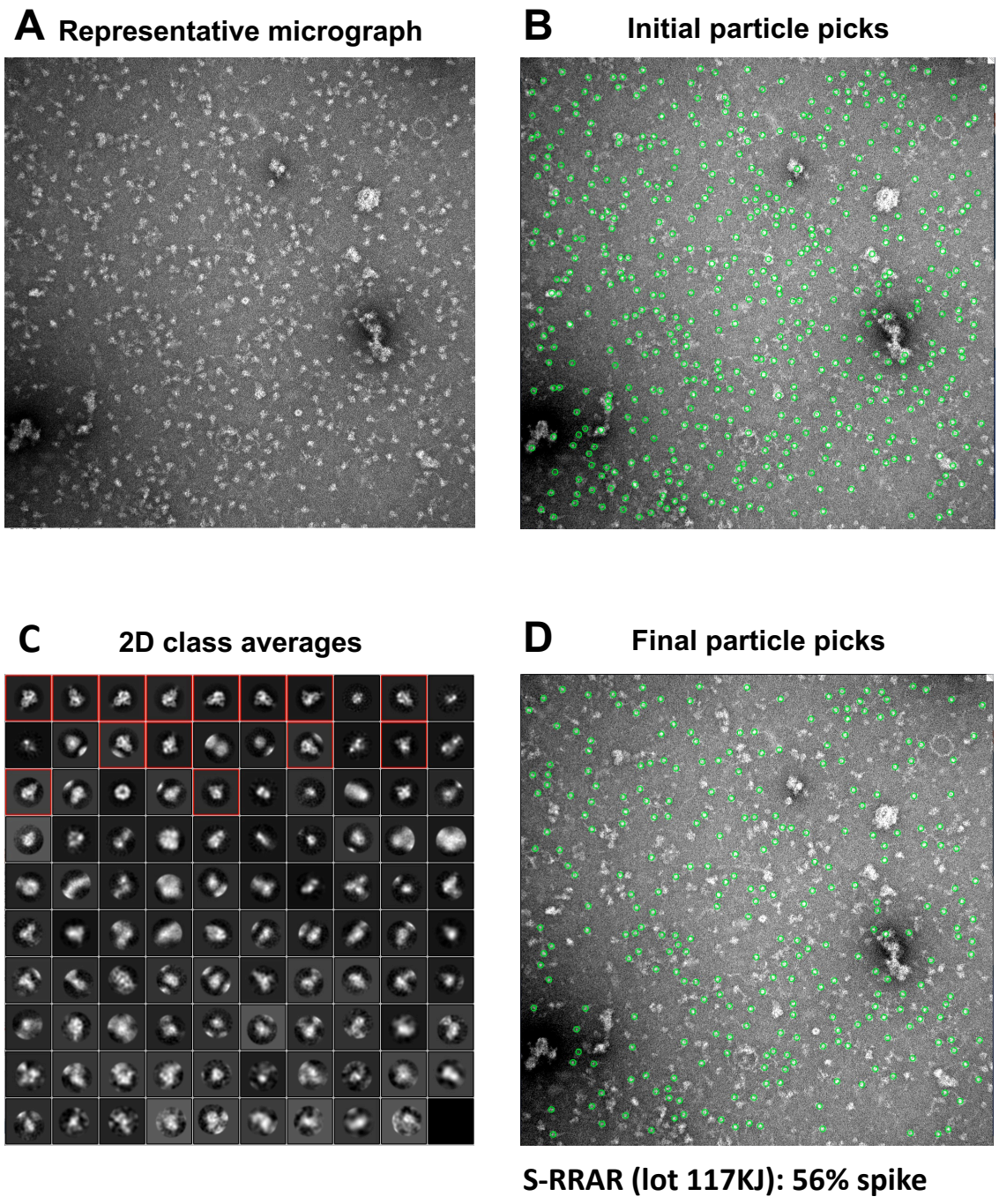

Data S5. NSEM and Cryo-EM data processing for the S-RRAR and S-RRAR/D614G SARS-CoV-2 S ectodomain, Related to Figure 6 and 7. A-D. S-RRAR NSEM. **A.** Representative NSEM micrograph. **B.** NSEM Particle picks in green. **C.** 2D class averages (the particles in the classes marked with a red box are recognizable as the pre-fusion spike). The rest of the classes are marked as "junk". **D.** NSEM Particles present in the boxed class averages in panel **C**. are shown with a green circle around them.

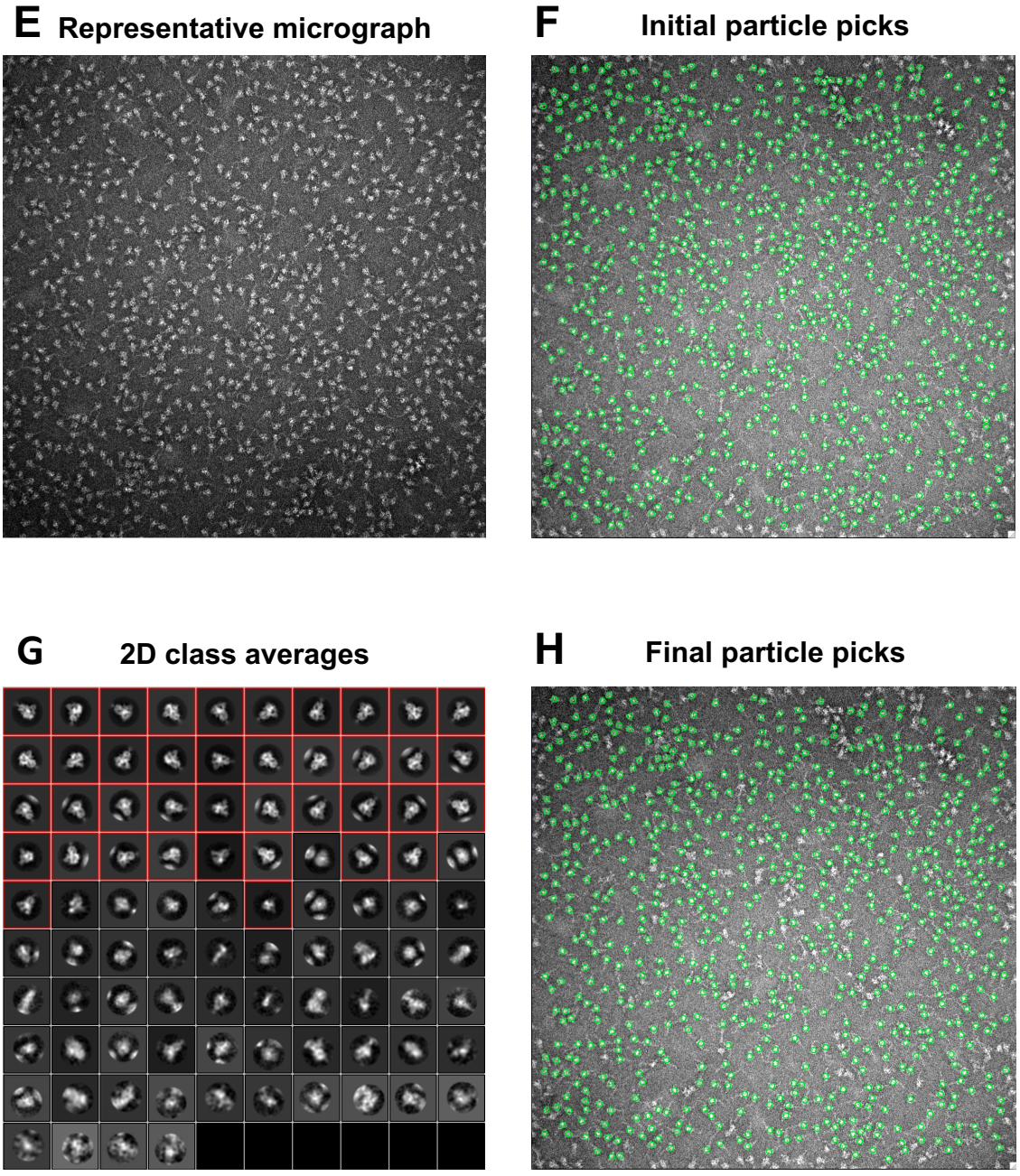

Data S5 continued. NSEM and Cryo-EM data processing for the S-RRAR and S-RRAR/D614G SARS-CoV-2 S ectodomain, Related to Figure 6 and 7. E-H. S-RRAR/D614G NSEM. **E.** Representative NSEM micrograph. **F.** NSEM Particle picks in green. **G.** 2D class averages (the particles in the classes marked with a red box are recognizable as the pre-fusion spike). The rest of the classes are marked as "junk". **H.** NSEM Particles present in the boxed class averages in panel **G**. are shown with a green circle around them.

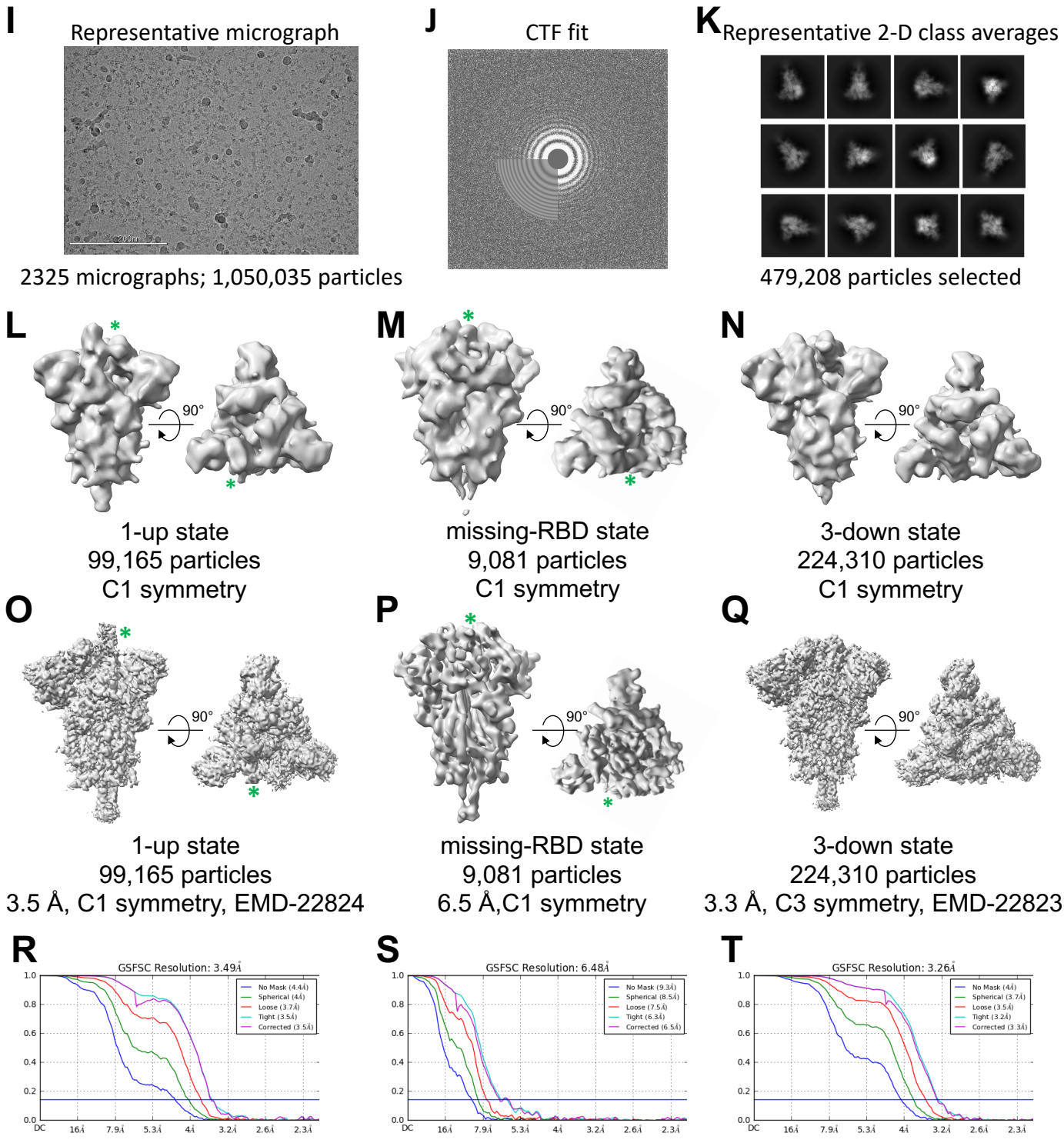

Data S5 continued. NSEM and Cryo-EM data processing for the S-RRAR and S-RRAR/D614G SARS-CoV-2 S ectodomain, Related to Figure 6 and 7. **I.** Representative cryo-EM micrograph for furin cleaved S-RRAR-D614G. **J.** Cryo-EM CTF fit furin cleaved S-RRAR-D614G. **K.** Representative 2D class averages from Cryo-EM dataset for furin cleaved S-RRAR-D614G. **L-N.** *Ab initio* reconstructions for the cryo-EM for furin cleaved S-RRAR-D614G **L.** 1-up state (the RBD in the up position is identified by an asterisk), **M**. missing-RBD state (the RBD in the up position or missing is identified by an asterisk) and **N.** 3-down state. **O-Q.** Refined maps for the cryo-EM for furin cleaved S-RRAR-D614G **O.** 1-up state (the RBD in the up position is identified by an asterisk) **P.** missing-RBD state (the RBD in the up position or missing is identified by an asterisk) and **Q.** 3-down state. **R-T.** Fourier shell correlation curves for the cryo-EM furin cleaved S-RRAR-D614G **R.** 1-up state, **S.** missing-RBD state and **T.** 3-down state.

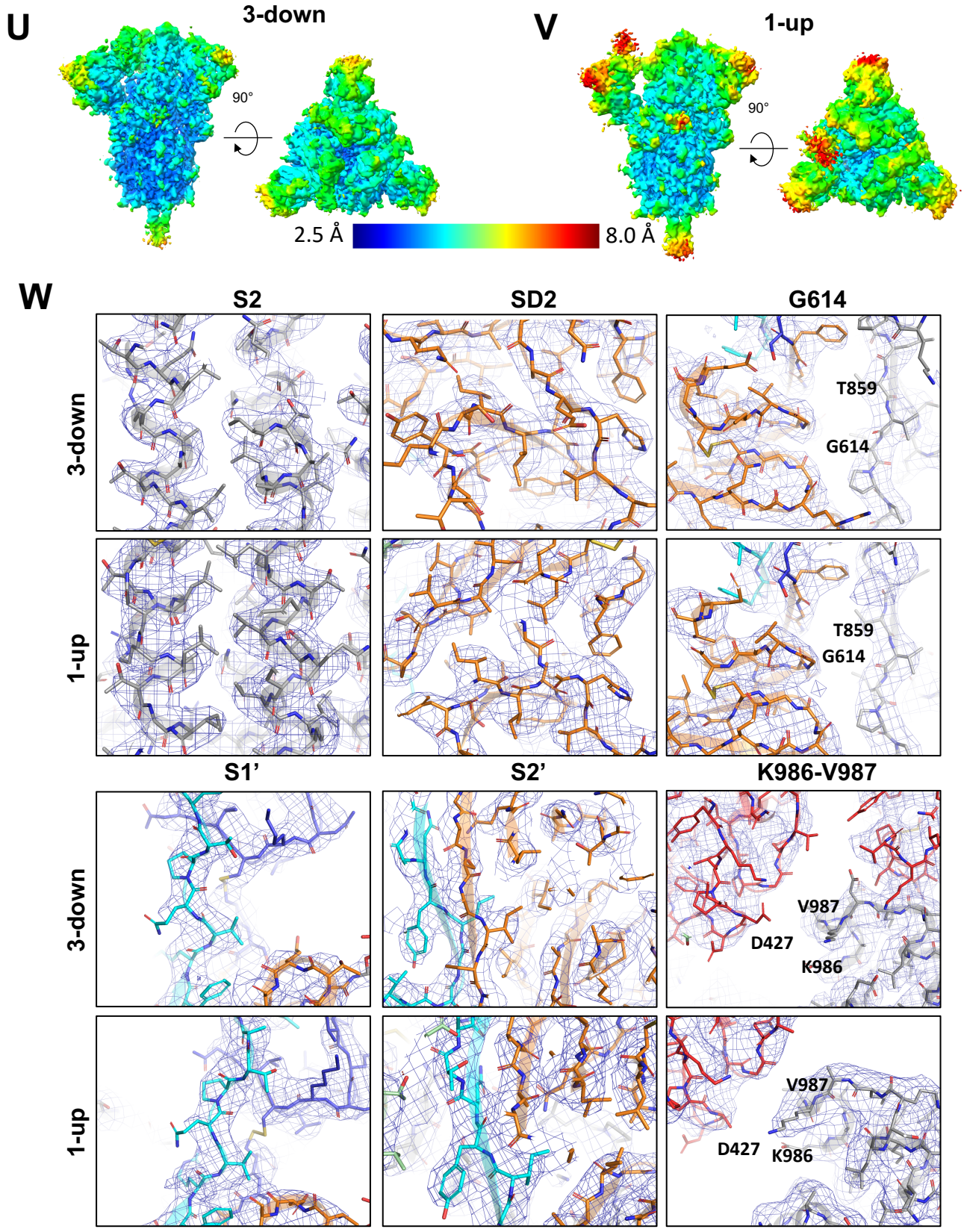

Data S5 continued. NSEM and Cryo-EM data processing for the S-RRAR and S-RRAR/D614G SARS-CoV-2 S ectodomain, Related to Figure 6 and 7. U-V. Refined cryo-EM maps colored by local resolution for the consensus **U.** 3-RBD-down (EMDB-22823) and **V.** 1-RDB-up (EMD-22824) states. **W.** Zoom-in images showing the S2, SD2, D614G, S1', S2' and K986-V987 regions in the consensus 3-RBD-down (top) and 1-RDB-up structures (bottom). The cryo-EM map is shown as a transparent surface and the fitted model is in cartoon representation, with residues shown as balls and sticks (PDB ID 7KDJ and 7KDI).

Data S5. NSEM and Cryo-EM data processing for the S-RRAR and S-RRAR/D614G SARS-CoV-2 S ectodomain, Related to Figure 6 and 7. A-D. S-RRAR NSEM. **A.** Representative NSEM micrograph. **B.** NSEM Particle picks in green. **C.** 2D class averages (the particles in the classes marked with a red box are recognizable as the pre-fusion spike). The rest of the classes are marked as "junk". **D.** NSEM Particles present in the boxed class averages in panel **C**. are shown with a green circle around them. **E-H.** S-RRAR/D614G NSEM. **E.** Representative NSEM micrograph. **F.** NSEM Particle picks in green. **G.** 2D class averages (the particles in the classes marked with a red box are recognizable as the pre-fusion spike). The rest of the classes are marked as "junk". **H.** NSEM Particles present in the boxed class averages in panel **G**. are shown with a green circle around them. **I.** Representative cryo-EM micrograph for furin cleaved S-RRAR-D614G. **J.** Cryo-EM CTF fit furin cleaved S-RRAR-D614G. **K.** Representative 2D class averages from Cryo-EM dataset for furin cleaved S-RRAR-D614G. **L-N.** *Ab initio* reconstructions for the cryo-EM for furin cleaved S-RRAR-D614G **L.** 1-up state (the RBD in the up position is identified by an asterisk), **M**. missing-RBD state (the RBD in the up position or missing is identified by an asterisk) and **N.** 3-down state. **O-Q.** Refined maps for the cryo-EM for furin cleaved S-RRAR-D614G **O.** 1-up state (the RBD in the up position is identified by an asterisk) **P.** missing-RBD state (the RBD in the up position or missing is identified by an asterisk) and **Q.** 3-down state. **R-T.** Fourier shell correlation curves for the cryo-EM furin cleaved S-RRAR-D614G **R.** 1-up state, **S.** missing-RBD state and **T.** 3-down state. **U-V.** Refined cryo-EM maps colored by local resolution for the consensus **U.** 3-RBD-down (EMDB-22823) and **V.** 1-RDB-up (EMD-22824) states. **W.** Zoom-in images showing the S2, SD2, D614G, S1', S2' and K986-V987 regions in the consensus 3-RBD-down (top) and 1-RDB-up structures (bottom). The cryo-EM map is shown as a transparent surface and the fitted model is in cartoon representation, with residues shown as balls and sticks (PDB ID 7KDJ and 7KDI).